

## REFERENCES

1. Wilson RF, Laxson DD, Christensen BV, McGinn AL, Kubo SH. Regional differences in sympathetic reinnervation after human orthotopic cardiac transplantation. *Circulation* 1993;88:165-171.
2. Kaye DM, Esler M, Kingwell B, McPherson G, Esmore D, Jennings G. Functional and neurochemical evidence for partial cardiac sympathetic reinnervation after cardiac transplantation in humans. *Circulation* 1993;88:1110-1118.
3. Kingwell BA, Thompson JM, Kaye DM, McPherson GA, Jennings GL, Esler MD. Heart rate spectral analysis, cardiac norepinephrine spillover, and muscle sympathetic nerve activity during human sympathetic nervous activation and failure. *Circulation* 1994;90:234-240.
4. Bernardi L, Bianchini B, Spadacini G, et al. Demonstrable cardiac reinnervation after human heart transplantation by carotid baroreflex modulation of R-R interval. *Circulation* 1995;92:2895-2903.
5. Guertner C, Krause BJ, Klepzig H Jr, et al. Sympathetic reinnervation after transplantation: dual-isotope neurotransmitter scintigraphy, norepinephrine content and histological examination. *Eur J Nucl Med* 1995;22:443-452.
6. Schwaiger M, Hutchins GD, Kalf V, et al. Evidence of regional catecholamine uptake and storage sites in the transplanted human heart by positron emission tomography. *J Clin Invest* 1991;87:1681-1690.
7. Dae MW, Marco TD, Botvinick EH, et al. Scintigraphic assessment of MIBG uptake in globally denervated human and canine hearts: implications for clinical studies. *J Nucl Med* 1987;28:1444-1450.
8. De Marco T, Dae M, Yuen-Green MSF, et al. Iodine-123 metaiodobenzylguanidine scintigraphic assessment of the transplanted human heart: evidence for late reinnervation. *Am J Coll Cardiol* 1995;25:927-931.
9. Hartmann A, Maul FD, Huth A, et al. Serial evaluation of left ventricular function by radionuclide ventriculography at rest and during exercise after orthotopic heart transplantation. *Eur J Nucl Med* 1993;20:146-150.

---

# Impact of Reorientation Algorithms on Quantitative Myocardial SPECT Perfusion Imaging

Mojgan Haddad and Gerold Porenta

Department of Cardiology, University of Vienna, Vienna, Austria

---

In myocardial SPECT perfusion imaging, reorientation algorithms from transaxial image planes are used to generate short- and long-axis views of myocardial tracer uptake. We performed phantom experiments with  $^{201}\text{Tl}$  to delineate how image reorientation affects the results of quantitative image analysis. **Methods:** Thirty consecutive patient studies were analyzed to characterize the distribution of the angle of reorientation in a clinical setting. Short-axis SPECT images of a cardiac phantom with and without a  $180^\circ$  cold-spot insert were reconstructed with three different backprojection filters (ramp, Metz and Butterworth) and reoriented through different angles ranging from  $45^\circ$  to  $89^\circ$ . Four interpolation algorithms were used to calculate from the transaxial images the pixel values of the reoriented images: (a) a simple interpolator that averages the pixel values of the eight neighboring pixels of the transaxial image; (b) a three-dimensional linear interpolator; (c) a hybrid interpolator that combines a two-dimensional linear in-plane with a one-dimensional cubic across-plane interpolation; and (d) a three-dimensional cubic convolution interpolator. Images were reoriented twice with opposite angles so that the original and the reoriented images could be directly compared. Circumferential profile analysis was applied to determine the root mean square error of corresponding profiles and the difference of the extent and the severity of perfusion defects. Single and multivariate analyses of variance (ANOVA) were used to compare the effects of the reorientation angle, the backprojection filter and the interpolation algorithm. **Results:** In the clinical studies, the angle between the transaxial and reoriented images was  $75^\circ \pm 10^\circ$  (s.d.). In 48 phantom experiments, multivariate ANOVA demonstrated that the backprojection filter and the interpolation algorithm significantly affect the circumferential profiles and the extent and severity of a perfusion defect ( $p < 0.05$ ). In contrast, the angle of reorientation was not a significant factor ( $p = \text{ns}$ ). By univariate analysis, the three-dimensional cubic interpolator was associated with significantly ( $p < 0.05$ ) less error than the simple and three-dimensional linear algorithms. Relative computation times (simple interpolator = 100%) were 119% for the three-dimensional linear, 136% for the hybrid and 243% for the three-dimensional cubic interpolator. **Conclusion:** For quantitative analysis of myocardial SPECT perfusion images, a Metz filter for filtered backprojection in combination with a three-dimensional cubic convolution interpolation for image reorientation appears to

offer improved accuracy.

**Key Words:** myocardial perfusion scintigraphy; SPECT image processing; quantitative image analysis; image reorientation

*J Nucl Med* 1998; 39:1864-1869

---

Myocardial SPECT perfusion scintigraphy is an established noninvasive technique to assess presence, severity and location of coronary artery disease. Quantitative analysis of SPECT perfusion images based on circumferential profile analysis and polar map display has been used to improve and standardize the diagnostic accuracy of tomographic cardiac perfusion imaging (1-4).

Image reconstruction by filtered backprojection generates images of myocardial tracer activity in transaxial image planes that are oriented perpendicular to the craniocaudal direction of the body. However, as the axis of the heart does not necessarily align with the body axis, standardized images of the cardiac anatomy need to be derived by reorienting transaxial planes into short- and long-axis views perpendicular to the axis of the heart (5,6).

Image reorientation involves a coordinate transformation from the coordinate system of the SPECT acquisition system into the intrinsic coordinate system of the heart, followed by an interpolation of tracer activities applied to the transaxial images. Thus, the pixel values of the activity distribution depicted on long- and short-axis views are obtained by filtered backprojection and pixel interpolation. Both algorithms result in image smoothing by low-pass filtering, which may introduce errors and thus affect quantitative image analysis (7-10).

Although the impact of image reconstruction has been characterized in previous studies (3), the effect of reorientation on quantitative SPECT images has not been delineated in detail. Descriptions of interpolation algorithms describe associated errors in general mathematical terms (8,11,12) but do not provide a detailed analysis tailored to SPECT perfusion imaging. Kuhle et al. (13) have reported the effects of image reorientation in cardiac PET imaging and demonstrated that reorientation algorithms differ with respect to the generation of

---

Received Aug. 6, 1997; revision accepted Jan. 28, 1998.

For correspondence or reprints contact: Gerold Porenta, MD, PhD, Department of Cardiology, University of Vienna, Währinger Gürtel 18-20, A 1090 Vienna, Austria.

artifacts. However, whether these results also apply to SPECT perfusion imaging remains undetermined.

The main purpose of this study was to investigate the influence of image reorientation algorithms with respect to artifactual alterations in the activity distributions of reoriented images. The distribution of the angle of reorientation in a clinical setting was determined from 30 consecutive patient studies. Cardiac phantoms were used to evaluate the impact of the reorientation angle, the reconstruction filter and the interpolation algorithm on the errors of circumferential profiles and the extent and severity of a simulated perfusion defect between the original and the reoriented images.

## MATERIALS AND METHODS

### Cardiac Phantoms

A commercially available cardiac phantom (Data Spectrum Co., Hillsborough, NC) was used to acquire the phantom images. The inner chamber of the phantom (diameter: 2 cm), which simulates the left ventricular cavity, was filled with water. The concentric outer chamber with a thickness of 1 cm, which represents myocardial tissue, was filled with water and 150  $\mu\text{Ci}$   $^{201}\text{Tl}$ -chloride. Perfusion defects were generated using a 2-cm-long cold-spot insert that covered a 180° arc. The cardiac phantom was immersed in a 20-cm-long water-filled cylinder to provide photon scatter.

### Image Acquisition and Reconstruction

Image acquisition was performed using a large-field-of-view, single-head SPECT gamma camera with a low-energy, medium-resolution, parallel-hole collimator (Apex 415, APC-3; Elscint, Haifa, Israel). The cardiac phantom was aligned parallel to the rotation axis of the gamma camera to ensure that short-axis images could be acquired directly as transaxial images without image reorientation. The camera head was rotated in continuous motion through a 180° arc from the right anterior oblique 55° to the left anterior oblique 125° position acquiring 30 projection images with a 64 × 64 image matrix and a pixel size of 6.8 mm. The average counting rate was 1 kct/sec.

The projection images were reconstructed into transaxial images using a zoom factor of 2 and one of three backprojection filters: a fifth-order Butterworth filter (cutoff frequency  $\omega_c = 0.25 \text{ cm}^{-1}$ , full width at half maximum (FWHM) = 12.2 mm), a third-order Metz filter (FWHM = 10.7 mm) and a ramp filter (FWHM = 8 mm). The values of FWHM were measured using a line source of  $^{201}\text{Tl}$  that was placed at the center of rotation at a distance of 30 cm from the camera head.

After image reconstruction, transaxial images were transferred from the gamma camera with its dedicated computer hardware to an image analysis workstation (Macintosh Quadra 700, Apple Computer, Inc., Apple Computer, Cupertino, CA). Image processing was performed using the public domain software package OSIRIS, a general image processing platform with a graphical user interface environment (available at the world wide web site: <http://expasy.hcuge.ch/www/UIN/UIN.html>). This academic software package was extended with additional software modules using C++ and object-oriented programming techniques (MPW; Apple, Inc.) to provide image reorientation with different interpolation algorithms and to permit image analysis by circumferential profiles.

### Image Reorientation

Because three-dimensional pixel coordinates of the transaxial images do not, in general, coincide with pixel coordinates of short- and long-axis images, derivation of standardized views involves coordinate transformation to be followed by interpolation of pixel values. The coordinate transformation is primarily determined by the spatial orientation of the long-axis of the heart and the location

and spacing of the reoriented image planes, as indicated by a human operator. Coordinate transformation was modeled as a sequence of image rotations and an image translation. The parameter values that specify the coordinate transformations were stored in a parameter file to permit the repetitive processing of images with equal parameter settings.

We compared four interpolation algorithms with respect to accuracy and computational efficiency ( $\hat{p}$  refers to the interpolated pixel value and  $p_i$  to the pixel value of data point  $i$  in the original images).

1. A simple interpolation method that calculates the average of the eight neighboring pixel values as:

$$\hat{p} = \frac{\sum_{i=1}^8 p_i}{8}. \quad \text{Eq. 1}$$

2. A three-dimensional linear interpolator that calculates the linear interpolation of the eight neighboring pixel values as:

$$\hat{p} = \sum_{i=1}^8 p_i (1 - d_x) \times (1 - d_y) \times (1 - d_z), \quad \text{Eq. 2}$$

where  $d_x, d_y, d_z \in [0,1]$  denote the relative distance in each direction between the calculated pixel location and the neighboring point.

3. A hybrid interpolator that combines in-plane two-dimensional linear interpolation with one-dimensional cubic convolution interpolation across planes as:

$$\hat{p} = \sum_{i=1}^4 \left( p_i^1 \times \prod_{i \neq j} \frac{(z - z_j)}{(z_i - z_j)} \right), \quad \text{Eq. 3}$$

where  $p_i^1$  is the interpolated pixel value in each plane obtained from the in-plane linear interpolation of neighboring points.

$$p_i^1 = \sum_{j=1}^4 p_j (1 - d_x) \times (1 - d_y), \quad \text{Eq. 4}$$

and  $z$  and  $z_i$  are the  $z$ -coordinates (across planes) of point  $p$  and the four interpolated in-plane points  $p_i$ , respectively.

4. A three-dimensional cubic convolution interpolator based on Catmull Rom interpolating curves implemented as sequential cubic interpolations in the X, Y and Z directions. The interpolation can be expressed by the following formula for each dimension:

$$I(u) = [t^3 \ t^2 \ t \ 1] \begin{bmatrix} -0.5 & 1.5 & -1.5 & 0.5 \\ 1.0 & -2.5 & 2.0 & -0.5 \\ -0.5 & 0 & 0.5 & 0 \\ 0 & 1 & 0 & 0 \end{bmatrix} \begin{bmatrix} u_1 \\ u_2 \\ u_3 \\ u_4 \end{bmatrix}, \quad \text{Eq. 5}$$

where  $I(u)$  is the interpolated value,  $\in [0,1]$  is a parameter that defines the fractional position between the point  $i$  and point  $i + 1$ , and  $u_1, u_2, u_3$  and  $u_4$  are four consecutive data points or interpolated values generated during the previous interpolation step. To calculate the final interpolated pixel value interpolations are performed in each direction for a cube of 4 × 4 × 4 data points. First, 16 interpolation steps are performed in the  $x$  direction using the 64 original pixel values. Then, four interpolations are conducted in the  $y$

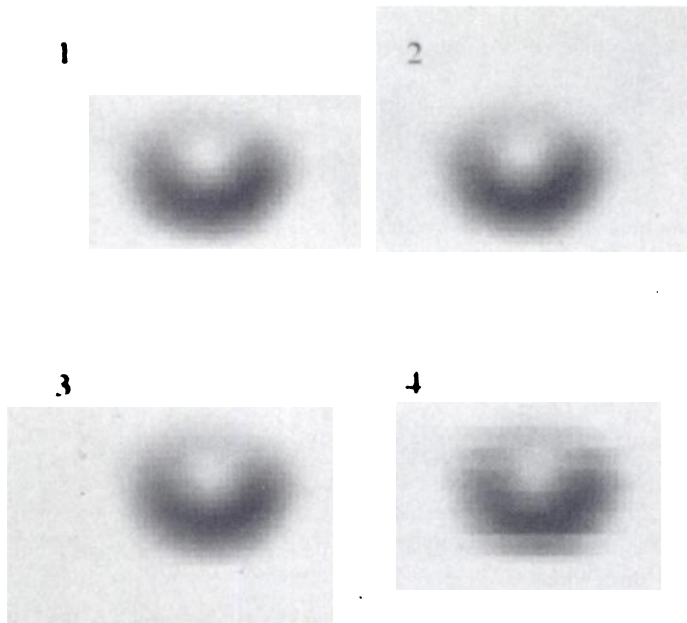


**FIGURE 1.** Phantom images reoriented twice in opposite directions using four different interpolation algorithms: (1) three-dimensional-cubic convolution interpolation, (2) hybrid interpolation combining two-dimensional-linear in-plane with one-dimensional cubic across planes, (3) three-dimensional-linear interpolator, and (4) simple interpolation scheme averaging pixel values of eight neighboring pixels.

direction using the 16 interpolated pixel values that were obtained with the first interpolation step. Last, an interpolation step in the z direction combines these four data points to generate the final interpolated pixel value.

Figure 1 displays sample phantom images that were reoriented using these four interpolation algorithms.

### Angle of Reorientation

To determine the distribution of the angle of reorientation in a clinical setting the angle between the axis of the body and the long-axis of the heart was measured in 30 consecutive patient studies. Phantom images were then reoriented through four different angles that were chosen to cover the estimated range of obliquity as determined in the clinical studies.

### Image Analysis

Phantom images were reoriented using each of the four interpolation algorithms with identical reorientation parameters. Two and four reorientation steps with equal angles in sequentially opposite directions were performed so that the circumferential profiles derived from the reoriented images could be directly compared with the circumferential profiles from the original images. Estimated values for a single interpolation step were calculated by linear regression analysis from the measured results obtained after two and four reorientation steps. After image normalization, radial profiles were searched for the maximal count activity along 60 rays at 6° intervals to obtain circumferential profiles. Profiles derived from original and reoriented images without a simulated perfusion defect were compared by calculating root mean square (RMS) errors. For profiles with a perfusion defect, the extent of the defect was determined by identifying all points on the circumferential profile with a relative count activity  $\leq 70\%$ . Severity of the perfusion defect was defined as the average decrease of the normalized count activity below 70% within the perfusion defect. Extent and severity of the defect in original and reoriented images were compared by calculating the unsigned normalized difference between respective values.

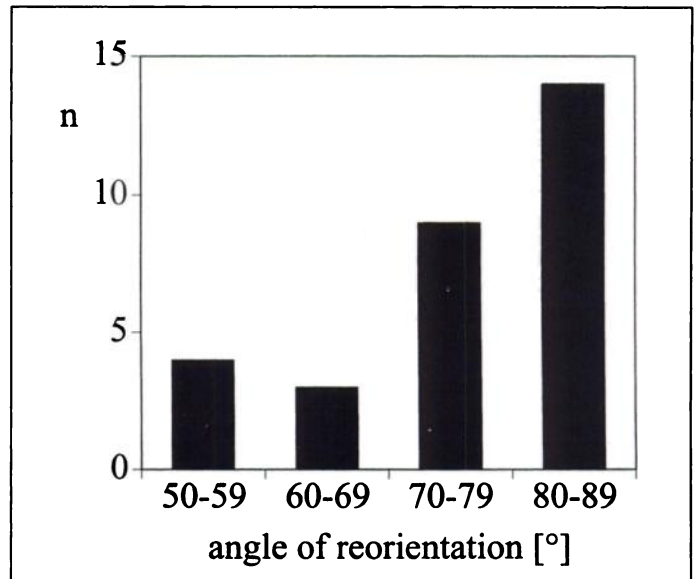


**FIGURE 2.** Distribution of angle of image reorientation subtended between craniocaudal direction of axis of body and long axis of heart, as measured in 30 patients.

### Statistical Analysis

Values given denote mean value  $\pm$  s.d. or mean value  $\pm$  s.e. as appropriate. Univariate and multivariate analyses of variance (ANOVA) were used to analyze the RMS error of circumferential profiles and the difference between extent and severity of the perfusion defect between original and reoriented images. Group comparisons were performed on the basis of Tukey-Kramer method with reorientation angle, reconstruction filter and interpolation algorithm as grouping variables. A  $p$  value  $< 0.05$  was considered to indicate statistical significance.

## RESULTS

### Angle of Reorientation

The distribution of the angle of reorientation subtended between the axis of the body and the long axis of the left ventricle as measured in 30 consecutive patients was  $75^\circ \pm 10^\circ$  (s.d.) and ranged from  $50^\circ$  to  $88^\circ$ , as shown in Figure 2. The effect of the reorientation angle on quantitative image analysis was then studied at angles of  $45^\circ$ ,  $60^\circ$ ,  $75^\circ$  and  $89^\circ$ , covering the expected range of angles observed in a clinical environment.

### Root Mean Square Errors of Circumferential Profiles

The normalized RMS error between circumferential profiles derived from the original and the reoriented images without a simulated perfusion defect was  $2.4\% \pm 1.0\%$  (range: 0.9%–6.4%). Multivariate ANOVA revealed that the normalized RMS error was significantly related to the reconstruction filter ( $p < 0.05$ ) and the interpolation algorithm ( $p < 0.005$ ), whereas the angle of reorientation did not show a significant effect ( $p = 0.34$ ).

When univariate ANOVA was used for group comparisons (Table 1), the Butterworth filter was associated with a significantly lower RMS error ( $p < 0.05$ ) than the ramp filter. Among the interpolation algorithms, the simple algorithm exhibited a significantly larger RMS error ( $p < 0.05$ ) than both the hybrid and the three-dimensional cubic algorithms. Also, the three-dimensional linear algorithm had a significantly higher RMS error than the three-dimensional cubic algorithm ( $p < 0.05$ ). There was no significant difference between the hybrid interpolator and either the three-dimensional linear or the three-dimensional cubic interpolation methods.

**TABLE 1**  
Normalized Root Mean Square Error (%) of Circumferential Profiles Between Original and Reoriented Phantom Images

Factor	n	Root mean square error (mean ± s.e.)	F ratio	p
Filter			5.18	< 0.01
Butterworth	16	1.9 ± 0.23		
Metz	16	2.2 ± 0.13		
Ramp	16	2.9 ± 0.30 <sup>†</sup>		
Interpolation			6.33	< 0.005
Three-dimensional cubic	12	1.7 ± 0.16		
Hybrid	12	2.0 ± 0.19		
Three-dimensional linear	12	2.5 ± 0.23 <sup>‡</sup>		
Simple	12	3.2 ± 0.37 <sup>‡§</sup>		
Angle			1.15	0.34
45°	12	1.9 ± 0.14		
60°	12	2.2 ± 0.43		
75°	12	2.6 ± 0.20		
89°	12	2.6 ± 0.29		

\*Grouped by reconstruction filter (Butterworth, Metz and ramp), interpolation algorithm (three-dimensional cubic, hybrid, three-dimensional linear and simple) and reorientation angle (45°, 60°, 75° and 89°). F ratios and p values were obtained from univariate analysis of variance, group comparisons were performed using the Tukey-Kramer method.

Significant differences (p < 0.05) between groups: <sup>†</sup> vs. Butterworth filter; <sup>‡</sup> vs. three-dimensional cubic interpolation; <sup>§</sup> vs. hybrid interpolation.

#### Extent and Severity of Perfusion Defects

Extent and severity of the simulated 180° perfusion defect on the original phantom images were 53% and 42%. The unsigned normalized differences of extent and severity of perfusion defects between the original and the reoriented images were 7.8% ± 8.6% (range: 0%–40%) and 20% ± 12% (range: 1%–51%), respectively. Multivariate ANOVA demonstrated significant effects of the reconstruction filter (p < 0.006) and the interpolation algorithm (p < 0.0001) on these differences.

By univariate ANOVA (Table 2), the Metz filter was significantly better than the Butterworth filter. Also, there was a trend for lower errors when the Metz filter was compared to the ramp

filter. Univariate ANOVA also revealed that the three-dimensional cubic interpolation was associated with significantly fewer errors (p < 0.05) in the characterization of the perfusion defect than both the three-dimensional linear and the simple interpolator. Moreover, although the hybrid interpolator was significantly better than the simple interpolator (p < 0.05), it was not different from the three-dimensional linear and the three-dimensional cubic interpolator. Yet, there was a trend for an improved accuracy of the three-dimensional cubic interpolation method when compared to the hybrid method. There was no statistically significant effect of the reorientation angle on the assessment of either extent or severity of the perfusion defect (p = ns). However, a trend for an increased error with increases in the reorientation angle was apparent.

#### Computational Complexity

For an entire operation of image reorientation that generates a set of reoriented short- and long-axis images from transaxial images, the relative computation time of the three-dimensional linear, hybrid and three-dimensional cubic interpolator when compared to the simple interpolation method (= 100%) were 119%, 136% and 243%.

#### DISCUSSION

This study sought to investigate the effects of the backprojection filter, the reorientation interpolator and the reorientation angle on quantitative image analysis of myocardial perfusion scintigrams. In most cases, quantitation of SPECT perfusion images uses circumferential profile analysis to assess regional myocardial tracer uptake or to characterize perfusion inhomogeneities by quantitating the extent and severity of perfusion defects.

SPECT image acquisition generates a set of projection images that are then submitted to image reconstruction and image reorientation to derive standardized short- and long-axis images for image analysis. However, both image reconstruction by filtered backprojection and image reorientation by coordinate transformation and pixel interpolation introduce smoothing artifacts into the images. For accurate SPECT quantitation, these artifactual alterations should be minimized by a proper

**TABLE 2**  
Unsigned Normalized Differences (̸) of Extent and Severity of Simulated 180° Perfusion Defect Between Original and Reoriented Phantom Images\*

Factor	̸ Extent mean ± s.e.	F ratio	p	̸ Severity mean ± s.e.	F ratio	p
Filter		5.2	< 0.01		1.9	0.17
Butterworth	11.8 ± 2.0			23.2 ± 3.4		
Metz	2.9 ± 0.8 <sup>†</sup>			14.9 ± 2.4		
Ramp	8.8 ± 2.7			18.8 ± 3.2		
Interpolation		9.2	< 0.0001		19.1	< 0.0001
Three-dimensional cubic	1.7 ± 0.5			7.2 ± 1.6		
Hybrid	4.3 ± 1.4			14.3 ± 2.6		
Three-dimensional linear	9.8 ± 2.0 <sup>‡</sup>			22.9 ± 2.6 <sup>‡</sup>		
Simple	15.5 ± 3.2 <sup>‡§</sup>			31.5 ± 2.8 <sup>‡§</sup>		
Angle		0.2	0.9		1.7	0.18
45°	6.4 ± 2.3			12.6 ± 2.4		
60°	7.3 ± 3.2			19.7 ± 3.7		
75°	8.3 ± 2.5			20.4 ± 2.7		
89°	9.3 ± 2.2			23.2 ± 4.7		

\*Grouped by reconstruction filter (Butterworth, Metz and ramp), interpolation algorithm (three-dimensional cubic, hybrid, three-dimensional linear and simple) and reorientation angle (45°, 60°, 75° and 89°). F ratios and p values were obtained from univariate analysis of variance, group comparisons were performed using the Tukey-Kramer method.

Significant differences (p < 0.05) between groups: <sup>†</sup> vs. Butterworth filter; <sup>‡</sup> vs. three-dimensional cubic interpolation; <sup>§</sup> vs. hybrid interpolation.

selection of reconstruction parameters and reorientation procedures.

### Angle of Reorientation

The angle of reorientation determines the amount of image rotation applied during coordinate transformation and thus affects the results of image reorientation. Although both the RMS error of circumferential profiles and the error in extent and severity of the perfusion defect did increase with increasing values of the reorientation angles, these effects did not reach statistical significance. In clinical practice, the angle of reorientation cannot be easily manipulated because the patient needs to be aligned with the rotating head of the gamma camera during image acquisition. Moreover, results from this study suggest that attempts to better align the axis of the camera with the long-axis of the heart rather than the axis of the patient's body will not have a major impact on quantitative image analysis and thus most probably do not require particular attention.

### Reconstruction Filter

An earlier study of quantitative image analysis of myocardial SPECT perfusion scintigrams (3) performed experiments to delineate the effect of backprojection filters on image quality and identified a fifth-order Butterworth filter as the optimal filter for quantitative polar map analysis. However, this study did not investigate the effects of the Metz filter, which was designed to offset resolution effects introduced by the imaging equipment. Among the three filters investigated in this study, the Butterworth filter was associated with the largest value of FWHM and thus with the most smoothing.

When the RMS error of circumferential profiles was analyzed, the Butterworth filter markedly reduced image noise and thus exhibited the lowest RMS error. However, when a simulated perfusion defect was analyzed, the smoothing not only reduced the contribution of noise but also introduced an additional error. In this setting, the Metz filter showed the lowest error values and appeared to adequately balance the opposing effects of noise reduction and preservation of spatial frequencies. These results suggest that for quantitative image analysis of perfusion defects, the Metz filter may offer slightly better accuracy than the Butterworth filter.

The design of this study, however, does not permit a comprehensive evaluation of the effect of filtering independent of an interpolation algorithm. The control images were generated by filtered backprojection, and no attempt was made to separately assess the effect of filtering by comparing reconstructed images to an assumed true count distribution. Therefore, the results of this study do not imply that any particular filter generally is associated with lower errors. Rather, the study suggests that for the quantitation of the extent and severity of perfusion defects, the combination of a Metz filter with a three-dimensional cubic interpolator provides the most accurate results.

### Interpolation Algorithm

Among the four interpolation algorithms investigated in this study, the three-dimensional cubic interpolator provided the best accuracy because it was associated with the lowest error values for both circumferential profile analysis and characterization of perfusion defects. However, the increase in accuracy was achieved at a significant cost in computation time.

Simple pixel interpolation, which is easy to implement, computationally fast but rather inaccurate, was included in this study to establish a reference level for comparisons with other more sophisticated interpolation methods. The errors associated

with the simple interpolator are not only reflected by poor performance in quantitative analysis but are also readily apparent by visual inspection of the images. Compared to the simple interpolator, the three-dimensional linear interpolator provided better image quality and smaller error values.

Linear interpolation may be inadequate when the spatial data sampling is anisotropic, and a hybrid interpolator that combines linear in-plane with cubic cross-plane interpolation may be better suited for pixel interpolation. In agreement with a previous study using PET phantoms (13), the hybrid interpolator was associated with smaller errors than the three-dimensional linear algorithm. However, in this study this effect did not reach statistical significance.

In general, the accuracy of the interpolation method increases with the increasing computational complexity of the algorithm (11,12,14). Accordingly, the three-dimensional cubic convolution interpolator that is based on a third-order algorithm to interpolate in plane and across planes showed the lowest error values. It remains undetermined whether a cubic spline interpolator or an interpolation scheme of an even higher order could significantly further reduce the errors. However, the requirements for computational resources would grow even further, and possible improvements can be expected to be small as error values already are low for the three-dimensional cubic convolution interpolation.

### Clinical Implications

Many commercially available SPECT systems currently use linear interpolation methods to generate reoriented short- and long-axis images of the heart from transaxial images. Migrating from three-dimensional linear interpolation to three-dimensional cubic convolution interpolation does increase computation time and thus may impact on patient throughput in a busy clinical environment. However, image reorientation comprises an only minor fraction of the total time required to completely analyze and fully document a myocardial perfusion study. Computation time increased twofold from three-dimensional linear to three-dimensional cubic convolution in this study. The difference can likely be reduced by optimizing the programming code. Moreover, the rapid growth of computing power offered by state-of-the-art microprocessor technology offsets the modest increase in computing time required by a three-dimensional cubic convolution interpolation, so that computation time should not impede the adoption of three-dimensional cubic convolution interpolation in clinical practice.

### CONCLUSION

This study demonstrates that the reorientation algorithm and the interpolation method significantly affect the accuracy of quantitative image analysis in myocardial SPECT perfusion imaging. Among the four interpolation algorithms, the three-dimensional cubic interpolator was associated with the smallest error values in all experiments. For quantitation of perfusion defects, a Metz filter for filtered backprojection in combination with a three-dimensional cubic convolution interpolation for image reorientation appear to offer improved accuracy.

### ACKNOWLEDGMENTS

We thank Brigitte Slama, Regina Wagner and Angela Fasching for technical assistance in performing the phantom experiments.

### REFERENCES

1. Garcia E, Van Train K, Maddahi J, et al. Quantification of rotational thallium-201 myocardial tomography. *J Nucl Med* 1985;26:17-26.
2. DePasquale E, Nody A, DePuey E, et al. Quantitative rotational thallium-201 tomography for identifying and localizing coronary artery disease. *Circulation* 1988;77:316-327.

3. Maddahi J, Train KV, Prigent F, et al. Quantitative single photon emission computed thallium-201 tomography for detection and localization of coronary artery disease: optimization and prospective validation of a new technique. *J Am Coll Cardiol* 1989;14:1689-1699.
4. Van Train KF, Maddahi J, Berman DS, et al. Quantitative analysis of tomographic stress thallium-201 myocardial scintigrams: a multicenter trial. *J Nucl Med* 1990;31:1168-1179.
5. ACC, AHA and SNM. Standardization of cardiac tomographic imaging. *J Nucl Cardiol* 1992;1:117-119.
6. O'Brien A, Gremmell H. Effectiveness of oblique section display in thallium-201 myocardial tomography. *Nucl Med Commun* 1986;7:609-616.
7. Metz C, Beck R. Quantitative effects of stationary linear image processing on noise and resolution of structure in radionuclide images. *J Nucl Med* 1975;15:164-170.
8. Carter W. Image sampling and interpolation. *SPIE* 1983;397:477-486.
9. King M, Schwinger R, Doherty P. Two-dimensional filtering of SPECT images using the Metz and Wiener filters. *J Nucl Med* 1984;25:1234-1240.
10. King MA, Glick SJ, Penney BC, Schwinger RB, Doherty PW. Interactive visual optimization of SPECT prereconstruction filtering. *J Nucl Med* 1987;28:1192-1198.
11. Shafer R, Rabiner L. A digital signal processing approach to interpolation. *Proc IEEE* 1973;61:692-702.
12. Maeland E. On the comparison of interpolation methods. *IEEE Trans Med Imaging* 1988;7:213-217.
13. Kuhle W, Porenta G, Huang H, Phelps M, Schelbert H. Issues in the quantitation of reoriented cardiac PET images. *J Nucl Med* 1992;33:1235-1242.
14. Keys R. Cubic convolution interpolation for digital image processing. *IEEE Trans Acoust, Speech, Signal Processing* 1981;29:1153-1160.

# Identification of Viable Myocardium in Patients with Chronic Coronary Artery Disease Using Rest-Redistribution Thallium-201 Tomography: Optimal Image Analysis

Leonardo Pace, Pasquale Perrone-Filardi, PierPaolo Mainenti, Alberto Cuocolo, Pasquale Vezzuto, Mariella Prastaro, Andrea Varrone, Giuseppe De Luca, Andrea Soricelli, Sandro Betocchi, Massimo Chiariello and Marco Salvatore  
*Cattedra di Medicina Nucleare, Dipartimento di Scienze Biomorfologiche e Funzionali, Facoltà di Medicina, Università Federico II, Napoli; Centro C.N.R. per la Medicina Nucleare, Napoli; and Cattedra di Cardiologia, Dipartimento di Medicina Interna, Facoltà di Medicina, Università Federico II, Napoli, Italy*

With the widely used 50% threshold, sensitivity is high, but specificity is low in detecting viable myocardium on  $^{201}\text{Tl}$  SPECT. In this study, we sought to identify the best threshold for semiquantitative  $^{201}\text{Tl}$  analysis. **Methods:** Rest-redistribution  $^{201}\text{Tl}$  SPECT was performed in 46 patients with chronic coronary artery disease before and after myocardial revascularization. Regional function was evaluated by two-dimensional echocardiography before and after myocardial revascularization using a 3-point scale (1 = normal, 2 = hypokinetic, 3 = a/dyskinetic). Myocardial segments with abnormal systolic function were defined as viable if the systolic function score decreased  $\geq 1$  after myocardial revascularization. A second group of 12 patients with chronic coronary artery disease constituted the validation population. Sensitivity-specificity curves, as well as receiver operating characteristic curves, for rest and redistribution images were generated by varying the  $^{201}\text{Tl}$  uptake threshold. **Results:** A 65% threshold uptake using resting images was found to be the best for detecting a/dyskinetic segments that improve after myocardial revascularization from those that do not improve. Sensitivity was lower with a 65% threshold (75%) than with a 50% threshold (90%,  $p < 0.05$ ), but specificity was higher (76% versus 26%,  $p < 0.05$ ) resulting in better accuracy (76% versus 57%,  $p < 0.05$ ) and positive predictive value (77% versus 55%), while the negative predictive value was not different (69% versus 75%,  $p$  not significant). The area under the receiver operating characteristic curve was significantly ( $p < 0.05$ ) larger for rest ( $0.80 \pm 0.05$ ) as opposed to redistribution ( $0.72 \pm 0.05$ ) images. Similar results were obtained in a subgroup of patients with low ejection fraction. Significant correlations between the percentage of revascularized viable segments and both the change in ejection fraction and in postrevascularization ejection fraction were found. When these findings were applied in the validation group, a gain in specificity, accuracy and positive predictive value was obtained with the 65% threshold compared with the 50% threshold. **Conclusion:** This

study demonstrated that analysis of resting images and use of the 65%  $^{201}\text{Tl}$  uptake threshold is preferable for separating viable from not viable dyssynergic myocardial segments in patients with chronic coronary artery disease.

**Key Words:** myocardial viability; thallium-201; thresholds

**J Nucl Med 1998; 39:1869-1874**

Thallium-201 is being used extensively to detect viable myocardium in patients with chronic coronary artery disease. Since the study (1) demonstrating that up to 50% of persistent  $^{201}\text{Tl}$  defects at 3-4 hr redistribution contain viable myocardium, modifications of the standard stress 3-4 hr redistribution approach have been proposed. Stress-redistribution-reinjection and rest-redistribution are the currently used protocols for the identification of viability using  $^{201}\text{Tl}$  (1-9). Interpretation of  $^{201}\text{Tl}$  images is enhanced by semiquantitative analysis of regional tracer uptake. In this analysis, a fixed cutoff is used to differentiate between viable and nonviable dysfunctional myocardium. Usually, a threshold value corresponding to 50% of maximal  $^{201}\text{Tl}$  uptake has been used, although the accuracy of such a cutoff to predict the effects of revascularization on regional function is not perfect and different values of sensitivity and specificity have been reported (9-14). Therefore, the aim of this study was to determine the most accurate analysis of resting  $^{201}\text{Tl}$  scintigraphy for identifying viable myocardium.

## MATERIALS AND METHODS

### Patient Population

Forty-six consecutive patients (45 men, 1 woman; mean age  $59 \pm 7$  yr) with chronic coronary artery disease and regional wall motion abnormalities at both angiography and echocardiography undergoing myocardial revascularization (25 patients underwent coronary artery bypass grafting and 21 patients underwent percutaneous transluminal coronary angioplasty) constituted the refer-

Received Oct. 6, 1997; revision accepted Jan. 26, 1998.

For correspondence or reprints contact: Leonardo Pace, trav.priv. Sanseverino 5/A, 80128, Napoli, Italy.